COO-3255-2

The decay of ^{161}Er to levels in ^{161}Ho†

J. L. Wood†† and D. S. Brenner

Jeppson Laboratory, Clark University, Worcester, Massachusetts 01610

Received 8 July 1971

Abstract: The gamma-ray spectrum of the decay chain ^{161}Er → ^{161}Ho → ^{161}Dy has been studied with Ge(Li) detectors. Results of γ-ray singles and coincidence experiments are reported and a decay scheme for ^{161}Er → ^{161}Ho is proposed. Asymptotic quantum-number assignments are made for several new energy levels in ^{161}Ho and the results are compared to predictions of the unified model. No evidence was found for the population of three-quasiparticle states in ^{161}Ho. De-excitation of the $3/2^-\{7/2^-[523],2^+\}$ γ-vibrational state and Coriolis coupling in the $1/2^+[411]$ rotational band are discussed.

E | RADIOACTIVITY ^{161}Er [from ^{161}Dy(α,4n)]; measured E_γ, I_γ, γγ-coin, $T_{1/2}$; deduced log ft. ^{161}Ho deduced levels, J, π, α_K, γ-multipolarities. Ge(Li) detectors.

† Work supported in part by the U.S. Atomic Energy Commission.

†† Present address: Institut für Angewandte Kernphysik, Kernforschungszentrum Karlsruhe, Karlsruhe, Germany.

DISCLAIMER

1. Introduction

In recent years the developments in the theoretical understanding of low-energy nuclear structure and in experimental equipment for nuclear spectroscopic studies have been considerable. Perhaps the most important ingredient necessary at this time for further progress in understanding nuclear structure is better experimental data on single-particle states and hence an improved knowledge of the average single-particle field[1]).

The level scheme of ^{161}Ho is one such case where improvements in the experimental data are possible. Early work on this nucleus was confined to investigation of the decay scheme of ^{161}Er using NaI(Tl) detectors[2]) and most recently in 1966 by Gromov et al[3]) using a magnetic spectrometer. The early work has been thoroughly summarised in ref. [3]) and is not repeated here.

Another experimental approach to understanding the level structure of ^{161}Ho has been made by two groups of experimenters in the past year. Rensfelt et al[4]) and Alonso et al[5]) at Stockholm and Yale, respectively, have measured the reaction γ-ray spectra of ^{161}Ho in-beam at accelerators. These experiments have provided a great deal of information about the rotational band built on the $7/2^-[523]$ ground state of ^{161}Ho and to a lesser extent about the band built on the 6.1 sec $1/2^+[411]$ isomeric state[6]).

In this paper we report our data on the γ-ray singles and coincidence spectra of ^{161}Er decay to ^{161}Ho obtained using high-resolution Ge(Li) detectors.

2. Source preparation, irradiations and chemical separation

Targets were prepared from Dy_2O_3 enriched[7]) to 90.0% isotopic abun-

dance in ^{161}Dy. The rare-earth oxide powder was slurried in an acetone-water solution on 30 mg/cm^2 aluminium backing foil and dried. The thickness of the deposit was typically about 5 mg/cm^2. Targets were covered with a 3 mg/cm^2 foil which served to contain the radioactive material during transport.

The ^{161}Er was produced by the ^{161}Dy(α,4n) reaction in the 41 MeV ^{4}He-ion beam of the Yale University heavy-ion accelerator. Beam currents were typically 0.7 μA and irradiation times about 7 h. Samples were returned to Clark University for chemical separation and counting.

At 40 MeV bombarding energy one expects[8,9] the predominant reactions to be (α,3n) and (α,4n) with significant contributions from (α,2n) and (α,p2n). Experimentally, the only radioactive rare-earth contaminants were 29-h ^{160}Er from ^{160}Dy(α,4n) and 63-min ^{162m}Ho from ^{161}Dy(α,p2n); ^{162}Er from ^{161}Dy(α,3n) is stable and 75-min ^{163}Er from the (α,2n) reaction decays through a 99.8% branch to the ground state of 33-y ^{163}Ho.

Radioactive contaminants arising from the aluminium foil and the oxide were removed by a simple chemical procedure. The irradiated Dy_2O_3 was dissolved in hot concentrated HNO_3, HCl was added and the solution heated for several minutes. The rare-earth elements were then precipitated as fluorides by the addition of a saturated solution of sodium fluoride. The resulting precipitate was centrifuged, washed and mounted on a sample card.

The delay between end of irradiation and start of γ-spectrum measurements was typically 2.5 h.

3. Source counting

Three Ge(Li) detectors were used in measurements of the singles and coincidence γ-ray spectra. A planar detector (5.5 cm^2 x 9 mm depletion depth) was used in the initial stages of this work to study the singles

spectrum. The detector gave a resolution of 3.0 keV FWHM at 1332 keV. Later measurements were made using a 33 cm^3 detector fabricated as a right circular cylinder with one open end, which gave a resolution of 2.2 keV FWHM. The better medium- and high-energy data were obtained with the large volume detector. Conventional pulse-shaping amplifiers and a 2048-channel pulse-height analyser were used in measuring the γ-ray spectrum.

Counting rates were kept at an optimum maximum of about 10^4 counts/sec by varying the source-to-detector distance. This maximised counting statistics without inpairing energy resolution. High-energy regions of the gamma-ray spectrum were studied with lead absorbers located between the source and detector to suppress low-energy contributions to the counting rate. The closest source-to-detector distance in the singles experiments was 1 cm. The incidence of summing between time-correlated γ-rays was estimated from spectra taken with and without lead absorbers.

Coincidence spectra were measured using the 33 cm^3 detector and a 15 cm^3 detector of similar design with 2.3 keV resolution. The detectors were positioned in a coaxial geometry during these experiments. The coincidence measurements were made with a fast-slow coincidence unit and a system of digital gates. Output pulses from the ADC of the gating detector were selected by setting digital windows on the spectrum regions of interest. Pulses from the other detector with the proper time relationship to the gating pulses (resolving time 70nsec) were selectively routed and stored in the memory of the pulse-height analyser. Typically, eight gates were set and eight 256-channel coincidence spectra were recorded in each experiment. In order to identify background contributions, off-peak gates were set for each peak. The spectrum from each background gate was then subtracted from the corresponding peak gate. The true/chance coincidence ratio for the system was about 60.

4. Gamma-ray energy and intensity measurements

The energy calibration was made using sources supplied by the International Atomic Energy Agency (IAEA): ^{241}Am, ^{57}Co, ^{22}Na, ^{137}Cs, ^{54}Mn, ^{88}Y, and ^{60}Co. Sources of ^{160}Tb, ^{109}Cd, ^{139}Ce, ^{192}Ir, ^{228}Th, ^{110m}Ag, ^{207}Bi, ^{65}Zn, ^{24}Na and ^{56}Co were also used. The 185.0 keV photopeak of the ^{182m}Ho present in the source was used as an internal standard[10]). The IAEA sources were also used as primary standards for construction of detector photopeak efficiency curves. Additional information about the shape of a curve was provided by fitting relative intensity measurements of gamma-rays from ^{160}Tb, ^{192}Ir, ^{152}Eu, ^{110m}Ag, ^{207}Bi and ^{56}Co to the curve determined by the IAEA standards.

The spectra were analysed in terms of energy and intensity by fitting a triangle to each experimental peak. A detailed description of this method has been given by Sugihara et al[11]). The apex of the fitted triangle defined the peak-channel number, and the area of the triangle was related to the relative gamma-ray intensity.

The energy corresponding to a channel number was obtained from the calibration-standard data as follows. Pairs of energy calibration peaks separated by approximately 1000 channels were used to determine a set of slopes for the energy calibration curve. An average slope computed from this set was used to define a linear calibration equation. The deviations of individual points from the linear fit were plotted on an expanded scale and used to determine a correction curve for counting-system nonlinearity. Each peak channel was corrected for system nonlinearity and the corresponding energy was calculated using the parameters of the linear equation. The errors quoted for photopeak energies incorporate errors in energy of the standards, the reproducibility of peak energies in two or more spectra measured with different detectors, the degree with which a peak is resolved from other photopeaks and the peak intensity with respect to the Compton background radiation.

Gamma-ray intensity error estimates include contributions from the

reproducibility of peak intensities in several measurements with different detectors, the error in the photopeak efficiency curves and absorber correction curves, error introduced when peaks were incompletely resolved from other photopeaks, and the uncertainty due to the background beneath a peak. The error in the photopeak efficiency curves took into account the varying source-to-detector distance during counting, source self-absorption and non-point counting geometries.

5. Half-life studies

Gamma-ray spectra recorded as a function of time following bombardment were used to assign peaks to the decay of ^{161}Er and to identify peaks arising from summing of γ-rays which were uncorrelated in time. The half-lives of the radioactive impurities, ^{160}Er and ^{162m}Ho, are sufficiently different from ^{161}Er for this method to work reliably for the more intense lines. To aid in identification of weak lines, sources of ^{160}Er and ^{162m}Ho were made and the γ-ray spectra measured. Contributions from these impurity activities were identified in the ^{161}Er spectra and removed from consideration. Some of these data have already been reported[12]). A similar procedure was followed to identify the γ-rays from 2.5-h ^{161}Ho decay which is present in equilibrium with ^{161}Er at the time of source counting. Further confirmation of the assignments was provided by studying the γ-ray spectra from α-particle bombardments of $^{161}Dy_2O_3$ at 22 and 32 MeV which emphasised the (α,2n) and (α,3n) reaction products.

The half-life of ^{161}Er was determined by following the gamma-decay of six intense lines: 94.1, 130.9, 211.1, 314.7, 592.7 and 826.6 keV. Data were collected over a period of six to eight half-lives in a number of experiments using different detectors and pulse-height analysers. The weighted mean value of the half-life for ^{161}Er determined in this manner

is 3.24 ± .04 h. The error estimate includes contributions from error in the intensity measurement of the photopeaks and the error over several determinations.

6. Results

Typical gamma-ray spectra over the energy range 20-2300 keV are shown in fig. 1. The energies of the peaks have been rounded to the nearest integer, and impurity lines are assigned where known. The results of the analyses for energy and intensity of ^{161}Er gamma-rays are summarised in table 1. Transitions in table 1 are encoded; for example, HD, where the letters refer to the initial and final levels, respectively, in ^{161}Ho as designated in fig. 4 and table 4.

The results of the coincidence experiments are found in table 2. Weak coincidences of questionable reliability are in parentheses. In order for a transition to be considered a strong coincidence, the peak in the coincidence spectrum had to be clearly distinguishable when compared with the background spectrum of the adjacent Compton gate. In addition the intensity relationships among lines seen in coincidence should be in agreement with the proposed decay scheme. An example of the coincidence spectra is found in fig. 2 where the γ-ray and background spectra in coincidence with the 932 keV transition are shown.

An attempt was made to make multipolarity assignments using our gamma-ray intensity data and the conversion electron intensity results of Gromov et al.[3]). The intensity scales were normalised to the theoretical value (ref. [13])) for an E3 assignment at 211.1 keV. Experimental conversion coefficients determined in this way are presented in fig. 3 and table 3. In many instances at energies above 600 keV it was difficult to determine the relationship between the electron and γ-ray data because of differences in the reported transtion energies and because of the poorer resolution of

the electron spectrum at high energies. In a number of cases there are three or four strong gamma-lines corresponding to each electron line. Therefore, we report only those conversion coefficients where the correspondence between the electron and γ-ray work is unambiguous. Where the conversion coefficient in table 3 is consistent with more than one assignment, the ambiguity is denoted, for example, (E1/E2) where we mean either E1 or E2. The assignment, M1, is not meant to preclude significant admixture of E2 character or vice versa.

The decay scheme proposed for ^{161}Er is shown in fig. 4. For the most part, the transitions we observe have not been seen in the previous decay studies[2,3]) or in the recent in-beam reaction γ-ray experiments[4,5]). A number of excited levels have been reported in the previous decay experiments but only three were firmly established in the scheme: 211.1, 592.7 and 826.6 keV. The decay scheme in fig. 4 is proposed on the basis of coincidence relationships, energy sums and intensity balances, multipolarity information and nuclear systematics. Transitions whose placement in the scheme is supported by the coincidence experiments are shown as filled circles; questionable data are shown as open circles. Levels are coded alphabetically for ease in presentation of the data. Levels which have been assigned to a definite rotational or vibrational band are designated sequentially. Under this notation the ground state rotational band is denoted A,B, the K-2 γ-vibrational band built on the ground state A',B' and the band built on the 211 keV level is designated; C, D, E, and F. Above 700 keV the coding is alphabetical with increasing excitation energy.

The scheme as presented in fig. 4 includes 141 of the 179 γ-rays assigned to ^{161}Er decay. Twelve transitions are assigned in two locations. Approximately 3% of the total γ-ray intensity is unassigned with a similar amount being assigned twice.

Log ft values for electron capture decay of ^{161}Er have been calculated

and are found in table 4 and fig. 4. The β-feed to each energy level was estimated from the intensity balance for the level. Care was taken to correct the γ-ray intensities for internal conversion and to include any uncertainty in multipolarity assignment i.e., M1/E2 mixing ratio, in the error estimate of the β-feed. The error associated with transitions which are assigned in more than one location in the scheme was accounted for by incorporating an uncertainty equal in magnitude to the sum of the intensities of the doubtful transitions. The β-feed to each level computed in this manner is found in table 4. Where there is no β-feed to a level within experimental uncertainty, no entry is made. The log ft values were computed from these data assuming there is no direct feed to the ground state of ^{161}Ho, using a Q_{EC} of 2050 keV (ref. 3) and our value of the ^{161}Er half-life. The effect of the unassigned γ-transitions in table 1 on the log ft computations will be considered in the discussion section.

7. The ^{161}Ho level scheme

In the following paragraphs, the properties of levels in ^{161}Ho are discussed individually or in groups where appropriate. The asymptotic quantum number assignments are summarised in fig. 5.

7.1 The ground-state rotational band

The ground-state rotational band built on the 7/2$^-$[523] Nilsson state is well established from the reaction spectroscopy work[4,5]. In our study there is no evidence for population of the band above the I = 9/2 member at 99 keV.

7.2 The 1/2$^+$[411] rotational band

The rotational band built on the 1/2$^+$[411] isomeric state at 211 keV has been partially characterised by the Stockholm work. Nuclear systematics

suggest that the spin 3/2 member of the rotational band is found about 10 keV above the band head (the exception being ^{165}Ho where the energy separation is 20 keV (ref. 14)). We propose that the 222 keV level in ^{161}Ho is the spin 3/2 member of the $1/2^+[411]$ band. The Stockholm group observed a 131 keV transition in ^{161}Ho which they assigned as the 7/2 → 3/2 crossover transition in the $1/2^+[411]$ band on the basis of cascade intensities and angular distribution data. We also see this transition and concur with their assignment which locates the 7/2 band member at 353 keV. From systematics of the $1/2^+[411]$ band energies and from de-excitation patterns of the high-energy levels it appears certain that the 5/2 member of the band is located at 316 keV. There is no evidence for population of any of the band members with $I > 7/2$ from ^{161}Er decay. Further discussion of the $1/2^+[411]$ band is deferred to section 8.4.

7.3 The $3/2^+[411]$ rotational band and the $7/2^+[404]$ band head

The 3/2, $3/2^+[411]$ and 7/2, $7/2^+[404]$ Nilsson states are expected to be close in energy to the 1/2, $1/2^+[411]$ state. This can be seen in fig. 6 where the experimental data on well-established single-quasiparticle states are plotted for the holmium isotopes and in fig. 7 where we present the results of calculations of Nilsson energy level diagrams for Z = 67, A = 161 (ref. 15)). The level at 253 keV is interpreted to be the $7/2^+[404]$ state because of its exclusive de-excitation to the spin 7/2 ground state. Further evidence for this assignment is the observation of a fairly intense 253 keV γ-ray in the reaction spectroscopy studies of both the Yale and Stockholm groups. Although neither group proposed an assignment for the 253 keV transition one would expect significant population of the $7/2^+[404]$ band in heavy-ion bombardments.

We assign the 299 and 373 keV levels in ^{161}Ho as the 3/2 and the 5/2 members of the $3/2^+[411]$ band. Strong support for the assignment of the

299 keV level as the $3/2^+[411]$ band head is the log ft value of 6.7 for electron capture feed which is consistent with a β-transition of the non-unique first-forbidden unhindered type ($\Delta I = 0, \pm 1$, $\Delta\pi$ = yes). Assignment of the 373 keV level as the 5/2 member of the $3/2^+[411]$ band requires the acceptance of a larger than usual energy spacing from the band head (usually about 55 keV).

7.4 The $K^\pi = 3/2^-$ γ-vibrational band

The level at 593 keV has been assigned in previous work[3]) as the K-2 γ-vibration superimposed on the $7/2^-[523]$ ground state. The strong E2 transition connecting this level with the ground state is the major evidence for this interpretation. The 649 keV level is assigned as the 5/2 member of the γ-band on the basis of multipolarity data, de-excitation patterns and rotational parameters. The values of $\hbar^2/2\mathcal{I}$ determined from the first two band members for the ground- and γ-bands in ^{161}Ho are 11.51 and 11.23 keV, respectively. For comparison, the same parameters in ^{165}Ho are 10.52 and 10.26 keV. The structure of the band-head is discussed in more detail in section 8.3.

7.5 The $5/2^-[532]$ band head

The level at 827 keV has been previously interpreted as the 5/2, $5/2^-[532]$ Nilsson state. The strong M1 transition connecting this level to the ground state together with the log ft value of 5.3 for β-feed from ^{161}Er supports this interpretation. It is interesting to note that the β-decay transition matrix element for $3/2,3/2^-[521] \rightarrow 5/2,5/2^-[532]$ comes under the recent classification of allowed-hindered transitions by

Fujita et al[16]). The log ft value of 5.3 is in agreement with their predictions.

7.6 The $1/2^-[541]$ rotational band

Multipolarity data require that the levels at 424 and 526 keV have negative parity. From fig. 7 it appears that the only low-lying negative parity states expected in ^{161}Ho are those of the $1/2^-[541]$ band. We suggest that the 424 keV level is either the spin 1/2 or 5/2 member of this band and that the 526 keV level is the 3/2 member. There are two difficulties with this interpretation: either the spin 1/2 or 5/2 member of the band appears to be missing, and the strong feed to the 526 keV level from the 1457 keV level does not appear to be matched by a comparably strong transition between the 1457 keV and 424 keV levels.

7.7 The $5/2^+[402]$ and $5/2^+[413]$ band heads

The levels at 447 and 760 keV appear to be single-quasiparticle states but the asymptotic quantum-number assignment of these states is somewhat unclear. The level at 447 keV is supported by the rather strong coincidence between the 447 and 1209 keV γ-rays. A 447 keV line was seen by the Stockholm group but was not assigned. The transition is E1 according to the conversion coefficient data, indicating positive parity for the 447 keV level. The existence of a level at 760 keV is based on the strong coincidence between the 253 and 508 keV γ-rays. The M1/E2 multipolarity of the 508 keV line determines positive parity for the 760 keV level. The decay patterns in ^{161}Ho suggest that both states have a spin $\leq 7/2$.

Consideration of figs. 6 and 7 leads us to propose that the 447 keV level is the 5/2, $5/2^+[402]$ Nilsson state and the 760 level is 5/2, $5/2^+[413]$. According to fig. 7 both states are expected below 1 MeV in

^{161}Ho although the calculations indicate that the $5/2^+[413]$ orbital should probably be lower in energy than $5/2^+[402]$. Experimental systematics indicate, however, that the $5/2^+[413]$ state is more likely to be found near 700 keV. There is little information on the location of the $5/2^+[402]$ orbital in light-mass rare-earth nuclei, although Ogle et al[17]) suggest that the ^{159}Tm ground state has this configuration.

7.8 The high-energy levels

Using the multipolarity data, log ft values and de-excitation patterns it was possible to assign spin and parity to several of the high-energy levels. These results are shown in fig. 4. The assignments should be regarded with caution because of the uncertainty in the high-energy multipolarity assignments.

8. Discussion

In this section we compare the ^{161}Er decay scheme with various aspects of nuclear theory. The items to be considered are the single-particle states, three-quasiparticle states, γ-vibrational states and Coriolis coupling.

8.1 The single-particle states

In fig. 7 are presented the results of a calculation of the single-

quasiparticle level energies for A = 161. The single-particle calculations were performed with the code of Nilsson et al[18]) by Wilhelmy[15]) using the parametric values $\kappa = 0.640$ and $\mu = 0.597$. The simple recipe without blocking was employed for the inclusion of the residual pairing force, using the correlation function and chemical potential as evaluated by Malov et al[19]). In general, the level ordering and energy scale is satisfactorily reproduced by the theory. One unfortunately experiences difficulty in trying to make finer comparisons between experiment and theory. For example, it is not possible to choose a combination of ε_2 and ε_4 values which simultaneously gives the correct level ordering for the 7/2[404], 1/2[541] and 5/2[402] orbitals in the scheme. We find therefore that the accuracy of the theory as presented here is insufficient to permit the use of the experimental level ordering as a device for estimating the values of ε_2 and ε_4 in ^{161}Ho. These orbitals, which vary rapidly in energy with changing ε_2 and ε_4, are a good test for future theoretical endeavours.

8.2 Complex and three-quasiparticle states

Soloviev and co-workers[20,21,22]) have made extensive calculations on the interactions of quasiparticles with collective vibrational phonons to give states of complex structure. Results of these investigations which are applicable to ^{161}Ho are found in table 5. Soloviev[23]) has also predicted the existence of three-quasiparticle states which are expected to occur at an excitation between 1 and 2 MeV in ^{161}Ho: those configurations which are expected to be populated in the decay of ^{161}Er are included in table 5.

It is evident from a comparison of the experimental results and the theoretical predictions in table 5 that a great deal remains to be learned

about nuclear structure. Our decay scheme work is not able to test the degree of admixture of orbitals in the states of complex structure. It is evident, though, that the experimental level ordering is not accurately predicted by the calculations.

One must also conclude from our experimental work that there is no evidence for the population of three-quasiparticle states in ^{161}Ho. According to Soloviev[23]) one might expect to find the allowed-unhindered (au) β-transitions: Er^{161} $3/2^-\{3/2^-[521]_n + 5/2^-[523]_n + 5/2^-[523]_n\} \rightarrow$ ^{161}Ho $1/2^-$ or $5/2^-\{3/2^-[521]_n + 5/2^-[523]_n + 7/2^-[523]_p\}$. Such states in ^{161}Ho should be recognisable by a log ft value <5.0 for β-feed from ^{161}Er. The lowest log ft value we find for an excited state above 1 MeV is 5.8 for level Y at 1657 keV. With this in mind one should consider the effect of the unassigned γ-rays in table 1. If the extreme assumption is made that all the unassigned γ-intensity were to de-excite level Y the effect is to lower the log ft to 5.4 which is too high a value for an au transition.

8.3 The $3/2^-\{7/2^-[523], 2^+\}$ vibrational state

From the point of view of the hydrodynamical model a K-2 γ-vibration should only de-excite to the single-quasiparticle state on which the vibration is superimposed. In ^{161}Ho, the $3/2^-\{7/2^-[523], 2^+\}$ state should only decay to the ground state. The existence of quasiparticle-phonon coupling can give rise to admixtures of other single-quasiparticle states and collective vibrations with the same spin and parity. This can cause more complex de-excitation patterns. Complex de-excitation patterns are also possible within the microscopic picture of collective vibrations.

The transitions observed between the γ-vibration at 593 keV (level A') and members of the $1/2^+[411]$ and $3/2^+[411]$ bands can be discussed in

terms of these theories. Assuming that the E2 transition A'A has a strength of 2.0 single-particle units (the corresponding transition in ^{165}Ho is 1.9 spu[24]), one can deduce the hindrance factors with respect to the Weisskopf estimate (ref.[25])) for the E1 transitions from A' to the [411] bands. They are: A'D, 5.9 x 10^4; A'E, 2.1 x 10^4; A'H, 3.8 x 10^4; and A'I, 2.6 x 10^4. These hindrance factors are typical for K-allowed E1 transitions between single-quasiparticle states in these nuclei.

One way to explain the transitions to the [411] bands is to postulate that the γ-vibration contains $K^{\pi} = 3/2^-$ components arising from collective octupole vibrations built on the $1/2^+[411]$ and $3/2^+[411]$ Nilsson states. Such collective modes probably occur at energies above 1200 keV in ^{161}Ho in view of the location of the 2^- and 1^- octupole band heads in ^{160}Dy at 1264 and 1288 keV[26], respectively. One expects that collective admixtures to the γ-vibration would be small because of the large energy separation between the states, but since admixed octupole components can have E1 strengths comparable to the single-particle ones such admixtures might be sufficient to explain the E1 transition probabilities to the [411] bands.

The γ-vibration may contain $3/2^-$ components from the $3/2^-[541]$, $3/2^-[532]$ and $3/2^-[521]$ single-quasiparticle states. Soloviev and Vogel[20]) calculate that the 593 keV state contains only 65% of the γ-vibration, with 12% $3/2^-[541]$ and the remainder unspecified (table 5). Although the energy denominator would appear to be large (ref. [17])) a $3/2^-[521]$ component seems a possibility and would de-excite to the $3/2^+[411]$ band by E1 transitions which are unhindered with respect to the asymptotic quantum numbers. The analogous transitions to the $1/2^+[411]$ band are hindered and this single-particle admixture would not explain their occurrence.

Bès and Cho[27]) have calculated the structure of the $3/2^-\{7/2^-[523], 2^+\}$ γ-vibration using a microscopic theory. The results relevant to the present discussion are summarised in table 6 and indicate that the dominant three-

quasiproton component of level A' is $3/2^-\{3/2^+[411]p, 1/2^+[411]p, 7/2^-[523]p\}$. De-excitation of the vibrational state can take place through E1 transitions such as: $3/2^-\{1/2^+[411]p, 5/2^+[413]p, 7/2^-[523]p\} \rightarrow 1/2^+\{1/2^+[411]p, 7/2^-[523]p, 7/2^-[523]p\}$ and $3/2^-\{3/2^+[411]p, 7/2^+[413]p, 7/2^-[523]p\} \rightarrow 3/2^+\{3/2^+[411], 7/2^-[523]p, 7/2^-[523]p\}$. These transitions are essentially $5/2^+[413] \rightarrow 7/2^-[523]$, a hindered E1 transition, and $7/2^+[413] \rightarrow 7/2^-[523]$; an unhindered E1 transition. On the basis of $(\text{amplitude})^2$ values for the components alone, the de-excitation to the $1/2^+[411]$ band should be about 30 times stronger than to the $3/2^+[411]$ band. One might expect, however, that this effect could be offset by the retardation of the $5/2^+[413] \rightarrow 7/2^-[523]$ transition relative to the $7/2^+[413] \rightarrow 7/2^-[523]$ transition because the former transition is hindered, an effect expected to produce a retardation of $\approx 10^4$ with respect to a competing unhindered E1 transition. Thus the microscopic picture is not inconsistent with the approximately equal population of the [411] bands from decay of level A'. A similar discussion of the $3/2^-$ gamma-vibrational band in ^{165}Ho has been presented by Reich and Bunker[28]).

8.4 Coriolis coupling in the $1/2^+[411]$ band

Rensfelt et al[4]) have located the $I + 1/2$ = even members of the $1/2^+[411]$ band up to $I = 23/2$ by assuming that the $I = 1/2$ and $I = 3/2$ members are separated by 10 keV. They also tentatively proposed the $I + 1/2$ = odd members between $I = 9/2$ and $21/2$ but the energies of these levels were not fixed relative to the band head. By combining the results of our decay scheme work with the reaction spectroscopy data it is possible to locate the entire band up to spin 23/2. In order for us to do this it is necessary to determine which γ-line of the Stockholm work is the $I = 9/2$ to $5/2$ transition since this transition was not identified in the decay scheme. An examination of the reaction spectroscopy data uncovers two potential candidates for this crossover transition: 204.2 and 208.8

keV. We select the 204 keV line as the better choice. Although the angular distribution coefficient $A_2/A_0 = -.04 \pm .14$ is not suggestive of an E2 transition, there is a large error associated with the measurement. On the basis of cascade intensity balance (ref. 4), the 204 keV γ-ray fits much better with the other members of the band. Also, a plot of the effective moment of inertia vs. I^2 (fig. 8) has a much smoother trajectory if the 204 keV line is chosen.

We have attempted in a crude way to extract parameters for the $1/2^+[411]$ band from fig. 8. An approximate fit to the $1/2^+[411]$ band is given by the following parameters: $A = 11.8$, $a = -.52$, in the formula

$$E(I,K) = E_K + A[I(I+1) + \delta_{K,1/2} a(-1)^{I+1/2}(I+1/2)]$$

It is apparent from the curvature of the lower envelope of the zig-zag plot that there is anomalous behavior in the rotational band. This curvature may result in part from Coriolis coupling arising from the close proximity of the $3/2^+[411]$ band. Bunker et al.[14]) have done a detailed analysis of the effect of the Coriolis interaction between these bands in ^{165}Ho where they also occur close in energy. They concluded that the anomalous decoupling parameter value for the $1/2^+[411]$ band in ^{165}Ho (-0.44; theoretical value, -0.88) could not be explained in terms of the expected Coriolis interaction with $3/2^+[411]$. In ^{161}Ho a complete band mixing calculation has not been done and is necessary in order to determine whether a similar anomaly exists.

9. Concluding remarks

A study of the decay scheme of ^{161}Er has given additional support for the qualitative understanding of low-energy nuclear structure in terms of the unified model. The detailed level structure of ^{161}Ho is not satisfactorily reproduced by calculations with the Nilsson scheme or by calculations of Soloviev and co-workers. In particular, no evidence was

found for the population of three-quasiparticle states in ^{161}Ho as predicted. Finally, the de-excitation pattern of the γ-vibration built on the ^{161}Ho ground state shows convincing evidence for departure from the hydrodynamic model. Three mechanisms which separately or taken together could explain the γ-ray branching are discussed although the data presented are not sufficient to prove or disprove any of the mechanisms.

The authors wish to thank Prof. R. Beringer, Prof. J. O. Rasmussen and the operating crew of the Yale University heavy-ion accelerator for their assistance in performing the irradiations. We extend our gratitude to Dr. J. Wilhelmy of the Lawrence Radiation Laboratory, Berkeley for the Nilsson level calculations and Prof. F. M. Bernthal of Michigan State University and Dr. M. E. Bunker of Los Alamos Scientific Laboratory for helpful comments.

References

1) V.G. Soloviev, Progress in Nuclear Physics, edited by D.M. Brink and J.H. Mulvey (Pergamon Press, London) 10 (1969) 239

2) H.A. Grench and S.B. Burson, Phys. Rev. 121 (1961) 831

3) K. Ya. Gromov, Zh. T. Zhelev, V. Zvolska and V.G. Kalinnikov, Sov. J. Nucl. Phys. 2 (1966) 559

4) K.-G. Rensfelt, A. Johnson and S.A. Hjorth, Nucl. Phys. A156 (1970) 529

5) J. Alonso, H. Bakhru, F.M. Bernthal, J. Boutet, B. Olsen, I. Rezanka and J.O. Rasmussen, Nucl. Phys. A160 (1971) 193

6) J.S. Geiger, R.L. Graham and M.W. Johns, Nucl. Phys. A161 (1971) 263

7) Obtained from the Isotopes Development Center, Oak Ridge National Laboratory

8) G.C. Martin, Jr. and R.C. Pilger, Jr., Nucl. Phys. 89 (1966) 481

9) J. Sau, A. Demeyer and R. Chery, Nucl. Phys. A121 (1968) 131

10) A. Bäcklin, A. Suarez, O.W.B. Schult, D.P.K. Maier, U. Gruber, E.B. Shera, D.W. Hafemeister, W.N. Shelton and R.K. Sheline, Phys. Rev. 160 (1967) 1011

11) T.T. Sugihara, J.A. Keenan and M.L. Perlman, Phys. Rev. 181 (1969) 1650

12) J.L. Wood and D.S. Brenner, Nucl. Phys. (1971) in press

13) R.S. Hager and E.C. Seltzer, Nucl. Data A4, nos. 1 and 2 (1968)

14) M.E. Bunker, G. Berzins and J.W. Starner, Contributed Paper, International Symposium on Nuclear Structure, Dubna, USSR (July 4-11, 1968)

15) J. Wilhelmy, Lawrence Radiation Laboratory, Berkeley (1971) private communication

16) J.-I. Fujita, G.T. Emery, and Y. Futami, Phys. Rev. C1 (1970) 2060

17) W. Ogle, S. Wahlborn, R. Piepenbring and S. Fredricksson, Rev. Mod. Phys. 43 (1971) 424

18) S.G. Nilsson, Chin Fu Tsang, A. Sobiczewski, Z. Szymański, S. Wycech, C. Gustafson, I.-L. Lamm, P. Möller and B. Nilsson, Nucl. Phys. A131 (1969) 1

19) L.A. Malov, V.G. Soloviev and I.D. Khristov, Sov. J. Nucl. Phys. 6 (1968) 863

20) V.G. Soloviev and P. Vogel, Nucl. Phys. A92 (1967) 449

21) V.G. Soloviev, P. Vogel and G. Jungklaussen, Izv. Akad. Nauk SSSR (ser. fiz.) 31 (1967) 518

22) V.G. Soloviev and P. Vogel, Sov. Phys. Doklady, 11 (1967) 940

23) V.G. Soloviev, Sov. Phys. JETP, 16 (1963) 176

24) R.M. Diamond, B. Elbek and F.S. Stephens, Nucl. Phys. 43 (1963) 560

25) J.M. Blatt and V.F. Weisskopf, Theoretical Nuclear Physics (Wiley, New York, 1952) 583

26) C. Gunther, H. Ryde and K. Krien, Nucl. Phys. A122 (1968) 401

27) D.R. Bes and Cho Yi-Chung, Nucl. Phys. 86 (1966) 581

28) C.W. Reich and M.E. Bunker, Bull. Acad. Sci. USSR, phys. ser. 31 (1967) 46

Table 1

Gamma-rays assigned to ^{161}Ho from decay of ^{161}Er

E_γ (keV)	I_γ [a]	Assignment [b]
77.0 ± 0.4	169 ± 37	HD
87.2 ± 0.7	53.6 ± 7.9	HC
94.1 ± 0.1	134 ± 11	ED
99.5 ± 0.6	64 ± 17	BA
109.9 ± 0.2	6.7 ± 1.4	
130.9 ± 0.2	88.7 ± 4.9	FD
147.8 ± 0.5	32 ± 19	LH
150.5 ± 0.6	5.5 ± 5.2	ID
152.4 ± 0.2	18.7 ± 2.4	KI
162.0 ± 0.2	4.9 ± 1.5	IC
201.4 ± 0.1	162 ± 8	JD
209.2 ± 1.0 [c]	140 ± 30	KE
211.1 ± 0.1	1820 ± 80	CA
219.5 ± 0.2	11.5 ± 1.8	A'I
236.3 ± 0.2	72.4 ± 3.2	
252.6 ± 0.2	69.1 ± 3.1	GA
276.0 ± 0.2	16.0 ± 1.8	A'E
294.0 ± 0.1	64.0 ± 3.2	A'H
303.4 ± 0.2	48.0 ± 3.2	KD
309.1 ± 0.3	10.7 ± 3.1	
314.7 ± 0.1	364 ± 15	KC
350.2 ± 0.3	12.2 ± 1.6	B'H
363.6 ± 0.4	9.0 ± 1.5	

370.7 ± 0.3	12.4 ± 1.6	A'D
376.4 ± 0.2	21.3 ± 1.8	OM
421.6 ± 0.3	56.7 ± 3.0	
446.8 ± 0.2	63.7 ± 4.5	LA
454.2 ± 0.4	7.5 ± 1.8	
467.8 ± 0.2	40.7 ± 2.5	
488.6 ± 0.4	12.9 ± 2.4	
499.0 ± 0.5	6.1 ± 2.4	QN
503.4 ± 0.5	5.5 ± 2.4	XO
507.5 ± 0.2	53.6 ± 3.8	MG
511.0 ± 0.1	35 ± 3[d]	$m_o c^2$
528.0 ± 0.2	60.6 ± 3.5	NH
549.4 ± 0.2	53.0 ± 3.6	B'B
554.2 ± 0.4	14.0 ± 3.2	aO
592.7 ± 0.1	594 ± 25	A'A
625.7 ± 0.4	14.1 ± 4.3	
648.9 ± 0.2	131 ± 9	B'A
662.5 ± 0.2	20.7 ± 3.4	
690.9 ± 0.2	52.7 ± 4.2	
719.1 ± 0.3	15:5 ± 2.5	
727.1 ± 0.2	142 ± 10	NB
737.2 ± 0.2	37.9 ± 3.4	
745.4 ± 0.5	7.9 ± 3.0	
747.7 ± 0.8	7.8 ± 2.9	SB'
767.1 ± 0.6	6.3 ± 2.8	
784.1 ± 0.4	8.7 ± 2.8	OF
799.4 ± 0.3	24.0 ± 3.9	QK
804.3 ± 0.2	50.1 ± 7.5	SA'
808.7 ± 0.2	56.4 ± 7.7	TB'

812.1 ± 0.2	73.0 ± 7.1	UB'
826.6 ± 0.1	10,000	NA
831.3 ± 0.5	14.8 ± 6.9	
839.4 ± 0.3	16.1 ± 3.4	VB'
842.1 ± 0.4	10.0 ± 3.4	WB'
859.2 ± 0.7	4.9 ± 2.9	
864.8 ± 0.2	214 ± 13	TA'
868.7 ± 0.3	55.4 ± 4.2	UA', RK
870.9 ± 0.5	12.6 ± 3.4	SK
875.7 ± 0.2	56.7 ± 4.6	
878.3 ± 0.4	36.5 ± 3.6	
880.8 ± 0.6	4.8 ± 3.7	XM
885.1 ± 0.7	8.1 ± 2.5	OG
895.6 ± 0.2	132 ± 8	VA'
898.2 ± 0.5	13.2 ± 3.1	WA'
904.4 ± 0.9	4.3 ± 2.6	
913.3 ± 0.9	3.3 ± 3.2	CN
923.0 ± 0.7	4.4 ± 2.2	PE
931.7 ± 0.2	309 ± 19	TK
935.6 ± 0.6	13.1 ± 4.0	UK
937.7 ± 0.6	11.2 ± 3.9	
940.9 ± 0.3	21.7 ± 2.6	PH
948.5 ± 0.6	40.5 ± 2.7	
951.3 ± 0.6	4.2 ± 2.7	QI
954.7 ± 0.6	4.6 ± 2.7	bM
962.4 ± 0.4	23.2 ± 3.4	VK
964.5 ± 0.9	4.9 ± 3.7	WK
970.3 ± 0.4	16.8 ± 3.0	RJ

973.0 ± 0.2	44.6 ± 3.7	SJ
980.2 ± 0.2	56.0 ± 4.1	CM
998.7 ± 0.2	26.2 ± 2.7	QE
1008.3 ± 0.6	6.2 ± 2.3	
1010.7 ± 0.3	15.3 ± 2.2	TL
1018.2 ± 0.5	5.1 ± 2.2	PD
1021.4 ± 0.4	12.7 ± 2.0	RI
1029.4 ± 0.6	5.4 ± 2.1	PC
1038.1 ± 0.5	8.4 ± 2.1	UJ
1047.6 ± 0.3	12.4 ± 1.8	XA'
1061.6 ± 0.5	9.9 ± 2.1	
1064.9 ± 0.3	17.6 ± 2.2	VJ
1078.0 ± 0.2	15.2 ± 2.0	RE
1088.5 ± 0.6	6.6 ± 1.8	UI
1098.3 ± 0.2	39.4 ± 3.2	eA', SH
1102.6 ± 0.3	32.1 ± 2.5	QD
1106.6 ± 0.6	4.1 ± 2.1	
1110.4 ± 0.6	4.7 ± 1.8	
1114.8 ± 0.6	7.7 ± 2.5	XK, VI
1118.0 ± 0.2	33.1 ± 3.1	WI
1145.3 ± 0.2	108 ± 7	UE
1147.6 ± 0.5	20.5 ± 3.6	cA'
1159.0 ± 0.2	82.3 ± 5.6	TH
1162.8 ± 0.5	3.5 ± 2.4	UH
1171.8 ± 0.2	56.8 ± 6.0	VE, RD
1174.7 ± 0.2	197 ± 12	WE, SD
1183.5 ± 0.4	49.1 ± 4.0	eA', RC
1185.8 ± 0.4	62.0 ± 4.6	SC

1189.7 ± 0.4	11.6 ± 2.3	VH
1193.3 ± 0.2	90.8 ± 5.9	WH
1199.4 ± 0.5	4.2 ± 1.8	
1202.4 ± 0.5	3.5 ± 1.8	
1209.9 ± 0.2	61.8 ± 4.2	YL
1228.3 ± 0.3	18.6 ± 2.2	ZL
1236.8 ± 0.9	2.5 ± 1.8	fA'
1239.0 ± 0.4	17.6 ± 1.8	UD
1247.1 ± 0.3	44.3 ± 3.7	
1250.3 ± 0.4	64.3 ± 4.4	eK, UC
1268.3 ± 0.2	36.5 ± 2.7	WD
1276.2 ± 0.4[e]	20.8 ± 3.2	hA'
1280.1 ± 0.2	89.8 ± 5.9	WC
1283.6 ± 0.9	3.7 ± 1.5	YI
1287.1 ± 0.5	5.3 ± 1.4	XF
1293.6 ± 0.6	3.3 ± 1.3	cL
1299.3 ± 0.6	3.3 ± 1.6	dL
1303.3 ± 0.4[e]	69.2 ± 4.6	YF
1313.9 ± 0.9	3.9 ± 1.5	
1318.3 ± 0.3	18.5 ± 2.3	aI
1324.8 ± 0.6	3.5 ± 1.1	XE
1333.3 ± 0.9	1.5 ± 1.2	
1338.2 ± 0.3	40.7 ± 4.0	aF
1341.2 ± 0.6	10.8 ± 3.6	bI, XH
1342.9 ± 0.6	8.1 ± 2.7	hK
1352.4 ± 0.6	3.1 ± 1.6	eJ
1358.3 ± 0.2	99.1 ± 7.1	YH
1361.4 ± 0.4	24.6 ± 3.4	bF

1371.8 ± 0.6	3.9 ± 1.7	dI
1374.9 ± 0.5	11.8 ± 2.3	aE
1377.0 ± 0.5	12.1 ± 2.1	ZH
1383.2 ± 0.2	21.5 ± 2.2	fL
1386.9 ± 0.4	8.0 ± 1.9	cF
1392.7 ± 0.2	13.0 ± 1.5	dF, aH
1404.4 ± 0.5	2.8 ± 0.9	YG
1417.8 ± 0.2	102 ± 7	XD
1421.1 ± 0.4	9.5 ± 2.4	
1425.2 ± 0.4	9.8 ± 1.9	
1429.1 ± 0.2	52.7 ± 3.7	dE, XC
1434.3 ± 0.2	32.7 ± 2.9	YD
1447.0 ± 0.4	4.9 ± 1.1	dH
1452.8 ± 0.2	7.6 ± 1.1	ZD
1456.4 ± 0.9	2.4 ± 1.5	fI, TA
1461.8 ± 0.4	18.8 ± 2.1	UA
1464.4 ± 0.3	40.2 ± 2.8	ZC
1468.9 ± 0.3	15.8 ± 1.5	aD
1477.7 ± 0.6	4.9 ± 1.7	eH
1480.4 ± 0.4	10.1 ± 2.0	aC
1488.3 ± 0.2	28.4 ± 2.2	VA
1492.1 ± 0.2	27.4 ± 2.1	bD
1495.2 ± 0.9	1.9 ± 1.2	hI
1517.7 ± 0.3	8.0 ± 1.2	
1523.8 ± 0.9	4.8 ± 2.5	dD
1525.2 ± 0.9	11.7 ± 6.0	
1527.6 ± 0.9	2.3 ± 1.5	
1531.2 ± 0.3	2.2 ± 1.1	gE, fH

1534.3 ± 0.3	2.3 ± 0.9	dC
1549.7 ± 0.9	1.2 ± 1.0	gH
1553.6 ± 0.2	25.3 ± 1.9	eD
1564.8 ± 0.3	2.3 ± 0.7	eC
1596.4 ± 0.4	2.2 ± 0.8	
1613.8 ± 0.3	2.8 ± 0.7	
1625.4 ± 0.4	2.0 ± 0.7	gD
1640.3 ± 0.3	3.3 ± 0.8	XA
1656.6 ± 0.2	88.6 ± 5.6	YA
1691.7 ± 0.9	1.2 ± 1.2	aA
1714.8 ± 0.5	4.8 ± 1.3	bA
1740.0 ± 0.2	64.1 ± 5.7	cA
1819.2 ± 0.9	1.0 ± 0.6	
1830.1 ± 0.5	8.6 ± 0.9	fA
1868.2 ± 0.7	2.5 ± 0.4	hA

---

a) Normalised to 10,000 at 827 keV

b) Letters designate energy levels involved in the transition as identified in fig. 4

c) Seen only in coincidence

d) Contains contributions from ^{162m}Ho and ^{160}Er decay

e) Wide peak, probably a multiplet

Table 2

Gamma-rays in coincidence from the decay of ^{161}Er

E_γ (keV)	Gamma-rays in coincidence with E_γ [a]
77.0	294.0
94.1	209.2, 931.7, 1145.3, 1174.7
99.5	727.1
130.9	1303.3, 1338.2
201.4	970.3, 973.0, (1064.9)
209.2	94.1, 931.7
252.6	507.5, (980.2)
314.7	(870.9), 931.7
592.7	(804.3), 864.8, 895.6
826.6	none
864.8	592.7
931.7	209.2, (303.4), 314.7
1174.7	94.1
1209.9	446.8

a) Questionable coincidences are in parentheses

Table 3

K conversion coefficients and multipolarities in ^{161}Ho

E_γ (keV)	α_K [a]	Multipolarity
130.9	3.5 ± 1.8 (-1) [b]	(E1/E2)
201.4	3.5 ± 1.5 (-2)	E1
211.1	4.6 ± 0.3 (-1)	E3
314.7	1.1 ± 0.2 (-2)	E1
421.6	6.3 ± 2.7 (-3)	E1
446.8	7.0 ± 2.8 (-3)	E1
507.5	1.9 ± 0.6 (-2)	M1/E2
592.7	8.8 ± 1.1 (-3)	E2
648.9	8.3 ± 1.8 (-3)	E2
812.1	4.7 ± 1.5 (-3)	E2
826.6	8.5 ± 0.6 (-3)	M1
864.8	4.0 ± 1.1 (-3)	E2
931.7	6.8 ± 1.6 (-3)	M1
1338.2	1.2 ± 0.5 (-3)	(E1/E2)
1358.3	6.9 ± 2.5 (-4)	E1
1417.8	1.8 ± 0.6 (-3)	M1/E2
1656.6	1.1 ± 0.4 (-3)	E2

a) Computed from the γ-ray intensities of this work and the conversion electron data of ref. [3]); see text for further details.

b) The entry 3.5 ± 1.8 (-1) is to be read $(3.5 \pm 1.8) \times 10^{-1}$.

Table 4

Log ft values and level assignments in ^{161}Ho

Energy (keV)	Code	I_β %	log ft	$K I^{\pi}[N\ n_z\ \Lambda]$
0	A	-	-	7/2, $7/2^-$ [523]
99.5 ± 0.2	B	-	-	7/2, $9/2^-$ [523]
211.1 ± 0.1	C	2.0 ± 4.0	>6.4	1/2, $1/2^+$ [411]
222.4 ± 0.2	D			1/2, $3/2^+$ [411]
252.6 ± 0.2	G	-	-	7/2, $7/2^+$ [404]
298.6 ± 0.2	H	4.8 ± 2.4	6.7 ± 0.3	3/2, $3/2^+$ [411]
316.4 ± 0.3	E	-	-	1/2, $5/2^+$ [411]
353.2 ± 0.2	F	-	-	1/2, $7/2^+$ [411]
373.3 ± 0.2	I	-	-	3/2, $5/2^+$ [411]
423.8 ± 0.3	J	0.5 ± 0.2	7.7 ± 0.2	1/2, $(1/2, 5/2)^-$ [541]
446.8 ± 0.2	L	-	-	5/2, $5/2^+$ [402]
525.8 ± 0.2	K	0.8 ± 0.4	7.4 ± 0.2	1/2, $3/2^-$ [541]
592.7 ± 0.1	A'	1.1 ± 0.5	7.3 ± 0.2	3/2, $3/2^-$ {7/2[523], 2^+}
648.9 ± 0.2	B'	0.2 ± 0.1	7.9 ± 0.3	3/2, $5/2^-$ {7/2[523], 2^+}
760.1 ± 0.3	M	-	-	5/2, $5/2^+$ [413]
826.6 ± 0.1	N	68.2 ± 0.2	5.3 ± 0.1	5/2, $5/2^-$ [532]
1137.0 ± 0.2	O	0.1 ± 0.1	7.9 ± 0.2	
1239.8 ± 0.2	P	0.2 ± 0.1	7.5 ± 0.1	
1325.1 ± 0.2	Q	0.6 ± 0.2	6.9 ± 0.1	
1394.4 ± 0.2	R	0.8 ± 0.5	6.7 ± 0.2	
1396.9 ± 0.1	S	2.0 ± 0.8	6.3 ± 0.2	
1457.5 ± 0.1	T	4.5 ± 0.3	5.8 ± 0.1	

1461.4 ± 0.1	U	2.1 ± 0.4	6.2 ± 0.2
1483.3 ± 0.1	V	1.7 ± 0.2	6.2 ± 0.2
1491.1 ± 0.2	W	2.5 ± 0.7	6.1 ± 0.2
1640.3 ± 0.1	X	1.1 ± 0.2	6.2 ± 0.2
1656.7 ± 0.1	Y	2.4 ± 0.2	5.8 ± 0.1
1675.3 ± 0.2	Z	0.5 ± 0.1	6.4 ± 0.1
1691.3 ± 0.1	a	0.8 ± 0.2	6.2 ± 0.2
1714.6 ± 0.2	b	0.4 ± 0.1	6.4 ± 0.2
1740.2 ± 0.1	c	1.0 ± 0.1	6.0 ± 0.1
1745.6 ± 0.2	d	0.3 ± 0.2	6.5 ± 0.2
1776.0 ± 0.2	e	0.6 ± 0.4	6.1 ± 0.2
1830.0 ± 0.3	f	0.2 ± 0.1	6.4 ± 0.2
1847.7 ± 0.3	g	0.03± 0.02	7.1 ± 0.2
1868.6 ± 0.3	h	0.2 ± 0.1	6.2 ± 0.1

Table 5

Complex and three-quasiparticle states in ^{161}Ho

K^{π}	Energy (keV)	Theoretical structure[a]
$7/2^-$	0	$523\uparrow$ 99 %
$3/2^+$	160	$411\uparrow$ 95 %
$1/2^+$	220	$411\downarrow$ 96 %
$5/2^+$	590	$413\downarrow$ 98 %
$7/2^+$	670	$404\downarrow$ 94 %; $(402\downarrow + 2^+)$ 4 %
$7/2^+$	850	$(411\uparrow + 2^+)$ 95 %; $413\uparrow$ 3 %
$5/2^-$	900	$532\uparrow$ 91 %
$3/2^-$	1000	$(523\uparrow + 2^+)$ 65 %; $521\uparrow$ 12 %
$1/2^+$	1000	$(411\uparrow + 2^+)$ 95 %; $411\downarrow$ 3 %
$11/2^-$	1050	$(523\uparrow + 2^+)$ 99 %; $505\uparrow$ 0.1 %
$9/2^-$	1100	$514\uparrow$ 99 %
$5/2^+$	1150	$(411\downarrow + 2^+)$ 97 %; $402\uparrow$ 2 %
$1/2^+$, $5/2^+$	1500	$\{3/2^-[521]_n, 5/2^+[642]_n, 7/2^-[523]_p\}$
$5/2^-$, $1/2^-$	1650	$\{3/2^-[521]_n, 5/2^-[523]_n, 7/2^-[523]_p\}$
$1/2^+$	1900	$\{3/2^-[521]_n, 3/2^-[521]_n, 1/2^+[411]_p\}$
$3/2^-$, $1/2^-$	1900	$\{3/2^-[521]_n, 5/2^+[642]_n, 1/2^+[411]_p\}$

a) Refs. [20,21,22,23]

Table 6

Microscopic structure of the $3/2^-\{7/2^-[523],2^+\}$ state[a])

Proton Orbitals	(amplitude)^2 %
$1/2^+[411]$, $3/2^+[411]$	29.4
$1/2^+[411]$, $5/2^+[413]$	9.4
$5/2^+[402]$, $9/2^+[404]$	2.3
$1/2^-[530]$, $5/2^-[532]$	1.1
$3/2^+[411]$, $7/2^+[413]$	0.3

a) Ref. [27]), only the major components of the three-quasiproton admixtures are listed

Fig. 1. Gamma-ray spectra from the decay of ^{161}Er. The data in fig. 1 were measured with the 33 cm^3 detector. The higher-energy spectra were obtained with a 1.4 g/cm^2 lead absorber located between the source and detector. The data in figs. 1a-b, 1c-d and in fig. 1e are from separate experiments. Peaks are labelled by energy rounded to the nearest keV. Impurity peaks from decay of ^{161}Ho, ^{162m}Ho and ^{160}Er are designated a, b and c respectively.

Fig. 2. Coincidence spectra from ^{161}Er decay. The upper portion of fig. 2 is the γ-ray spectrum in coincidence with the 932 keV photopeak. The lower portion is the spectrum in coincidence with a gate of equal width set on the Compton background at slightly higher energy.

Fig. 3. Theoretical (ref.[13])) and experimental values of the K-conversion coefficients of some transitions in ^{161}Ho. The conversion electron data of ref.[3]) have been combined with our gamma-ray data to obtain the experimental points.

Fig. 4. Level scheme of ^{161}Ho as seen in the decay of ^{161}Er. Energies are in keV and relative γ-ray intensities are shown in parentheses. Transitions whose assignments are confirmed by coincidence data are marked with a filled circle. An open circle is used to indicate that the coincidence is questionable. To the left of each level is shown the I^{π} assignment, if any, and to the right the log ft value for electron capture decay. Letter designations are explained in the text.

Fig. 5. Asymptotic quantum number assignments in ^{161}Ho.

Fig. 6. Experimentally observed Nilsson single-quasiparticle states in the odd-A holmium isotopes.

Fig. 7. Theoretical predictions for single-proton levels in ^{161}Ho. The energy level scheme was calculated using the Nilsson code (ref.[18]) and corrected for pairing using the parameters of ref.[19]). The experimental level scheme is included for comparison.

Fig. 8. Plot of effective inverse moments of inertia associated with individual cascade transitions in the $1/2^+[411]$ band in ^{161}Ho. The data of ref.[4]) were used to construct the band above spin 7/2. The numbers shown on the abscissa are values of I.

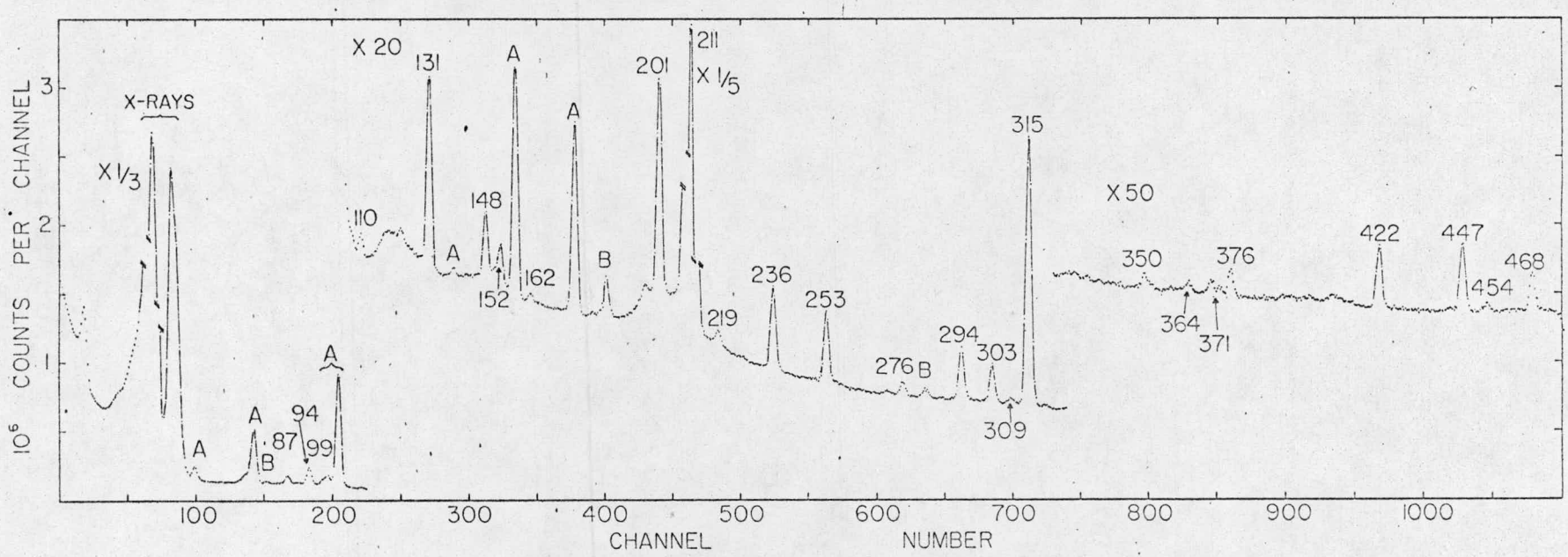
X-RAYS
X 1/3
X 20
X 1/5
X 50
A
B
87
94
99
110
131
148
152
162
201
211
219
236
253
276
294
303
309
315
350
364
371
376
422
447
454
468
10⁶ COUNTS PER CHANNEL
CHANNEL NUMBER
100
200
300
400
500
600
700
800
900
1000
1
2
3

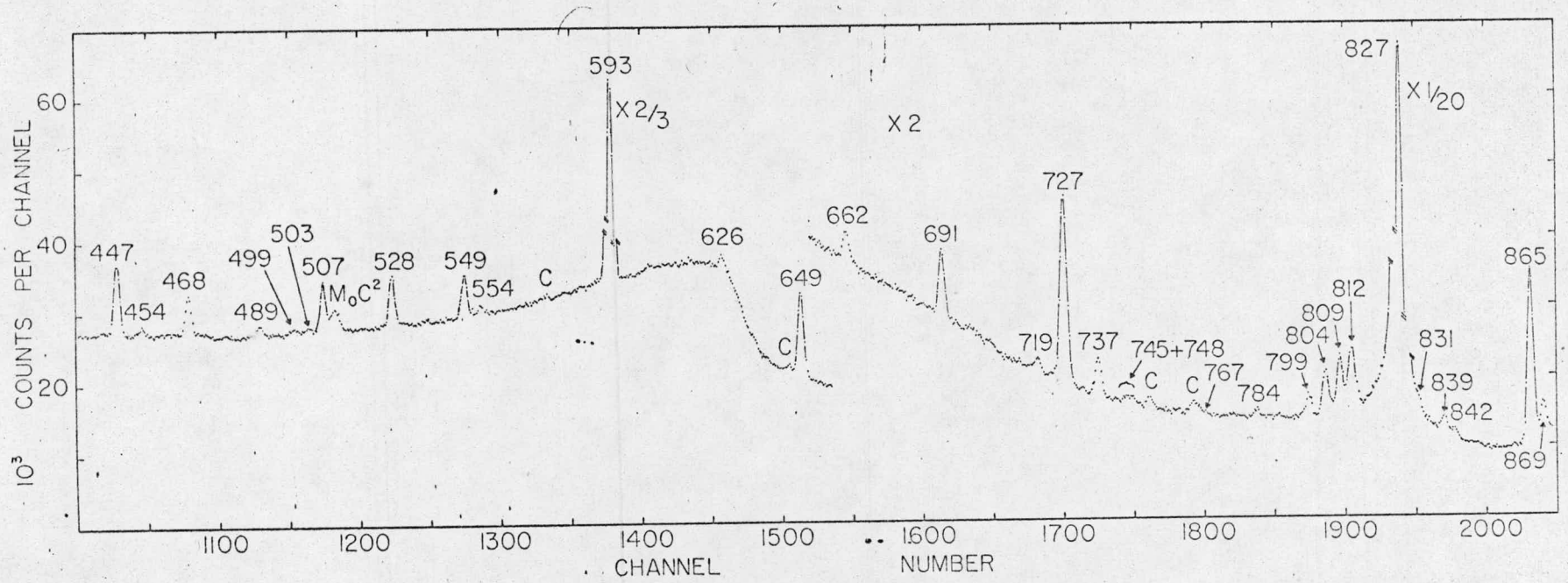
10³ COUNTS PER CHANNEL
60
40
20
1100
1200
1300
1400
1500
1600
1700
1800
1900
2000
CHANNEL NUMBER
447
454
468
489
499
503
507
M_0C^2
528
549
554
C
593
X 2/3
626
649
C
662
691
727
719
737
745+748
C
C
767
784
799
804
809
812
827
X 1/20
831
839
842
865
869
X 2

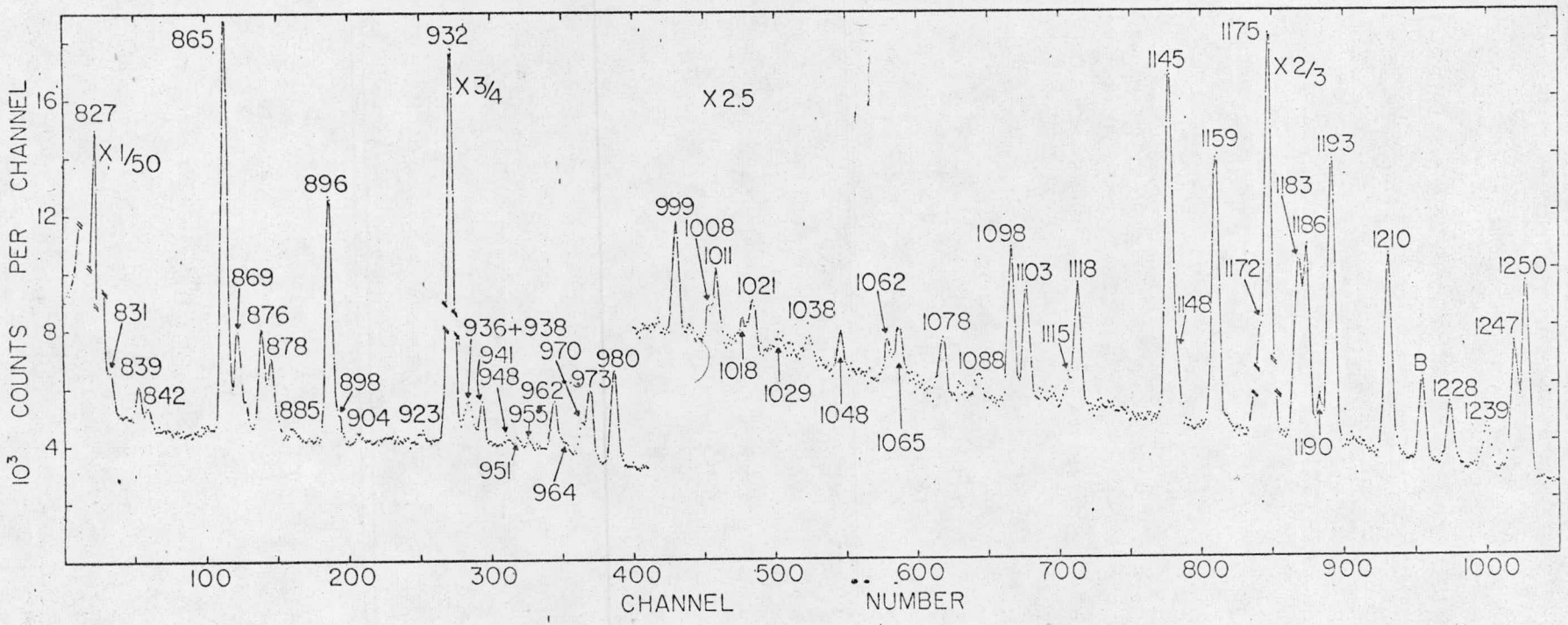
827
X 1/50
865
869
876
878
885
896
898
904
923
932
X 3/4
936+938
941
948
951
955
962
964
970
973
980
X 2.5
999
1008
1011
1018
1021
1029
1038
1048
1062
1065
1078
1088
1098
1103
1115
1118
1145
1148
1159
1172
1175
X 2/3
1183
1186
1190
1193
1210
B
1228
1239
1247
1250
842
831
839
10^3 COUNTS PER CHANNEL
16
12
8
4
100
200
300
400
500
600
700
800
900
1000
CHANNEL NUMBER

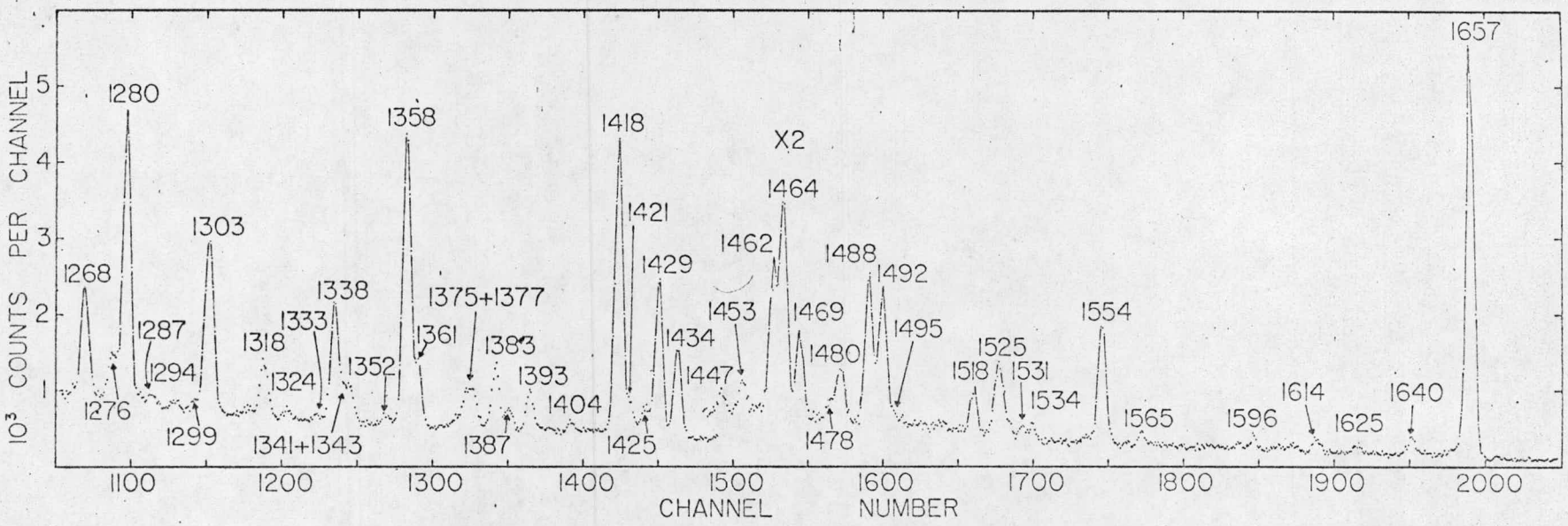
10³ COUNTS PER CHANNEL
1
2
3
4
5
1100
1200
1300
1400
1500
1600
1700
1800
1900
2000
CHANNEL NUMBER
1280
1268
1303
1358
1418
X2
1464
1421
1462
1429
1488
1492
1338
1333
1375+1377
1453
1469
1554
1287
1318
1361
1434
1495
1294
1324
1352
1383
1480
1525
1518
1531
1393
1447
1534
1404
1614
1640
1276
1299
1341+1343
1387
1425
1478
1565
1596
1625
1657

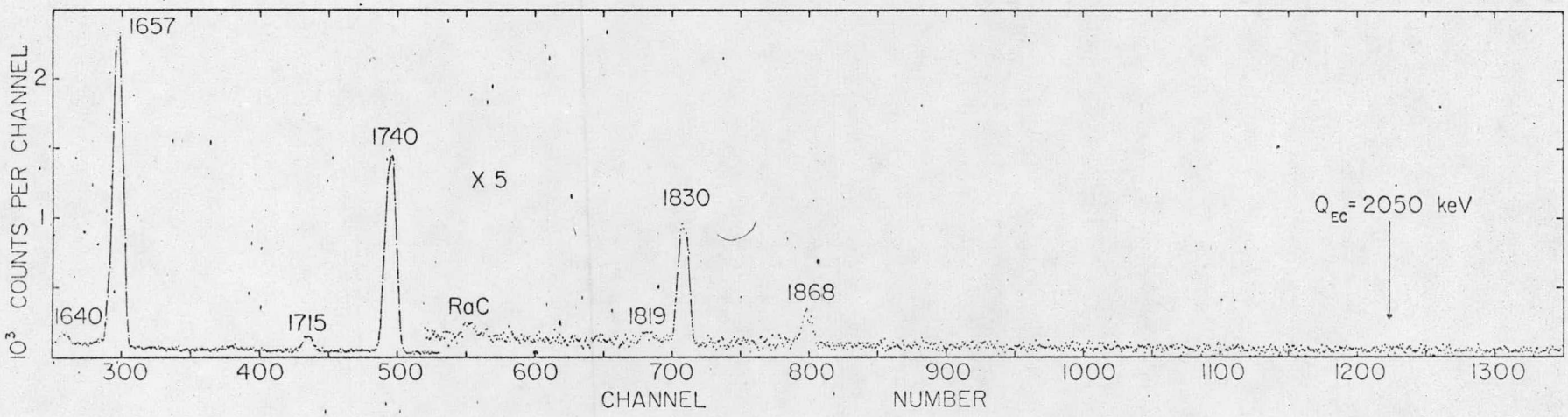
1657
1740
X 5
1830
Q_{EC} = 2050 keV
1640
1715
RaC
1819
1868
10^3 COUNTS PER CHANNEL
2
1
300
400
500
600
700
800
900
1000
1100
1200
1300
CHANNEL NUMBER

Fig 1 e

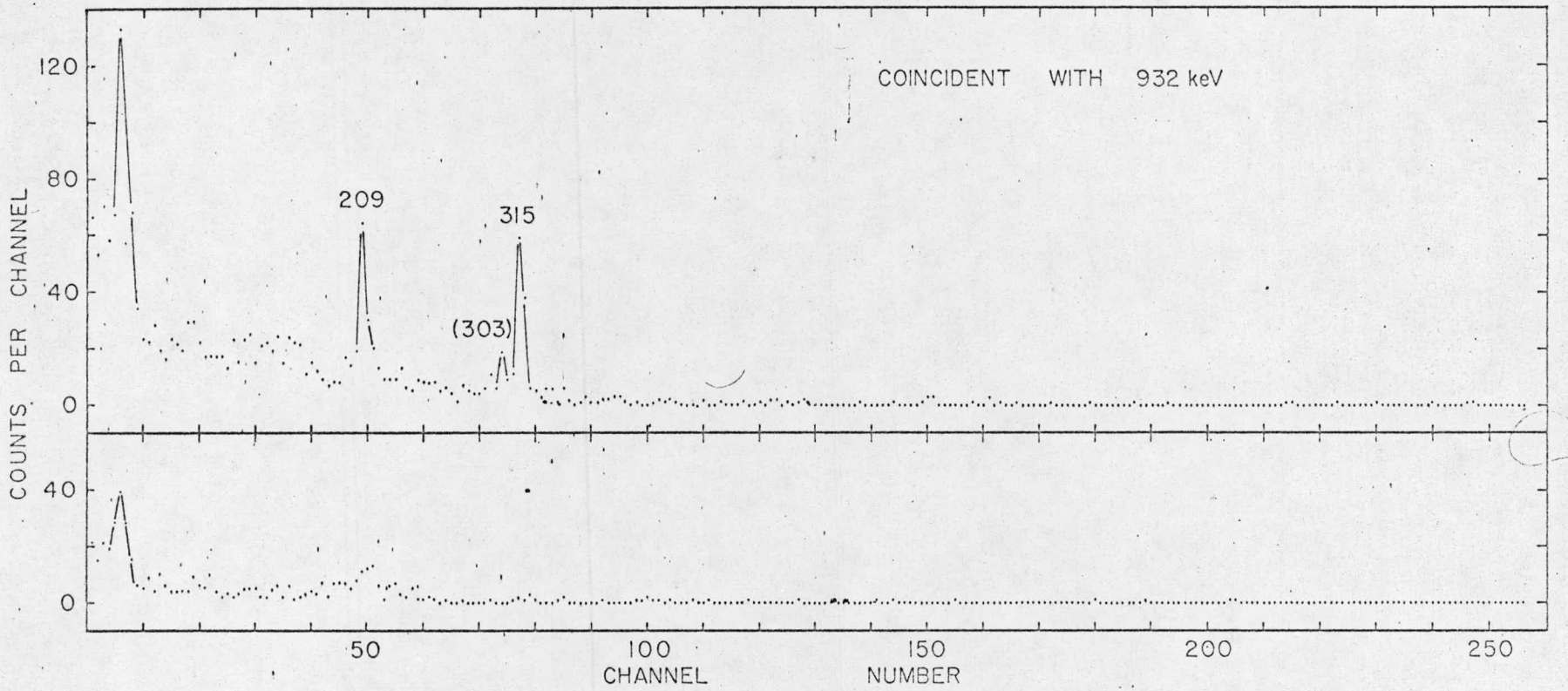
COINCIDENT WITH 932 keV
209
315
(303)
120
80
40
0
40
0
COUNTS PER CHANNEL
50
100
150
200
250
CHANNEL NUMBER

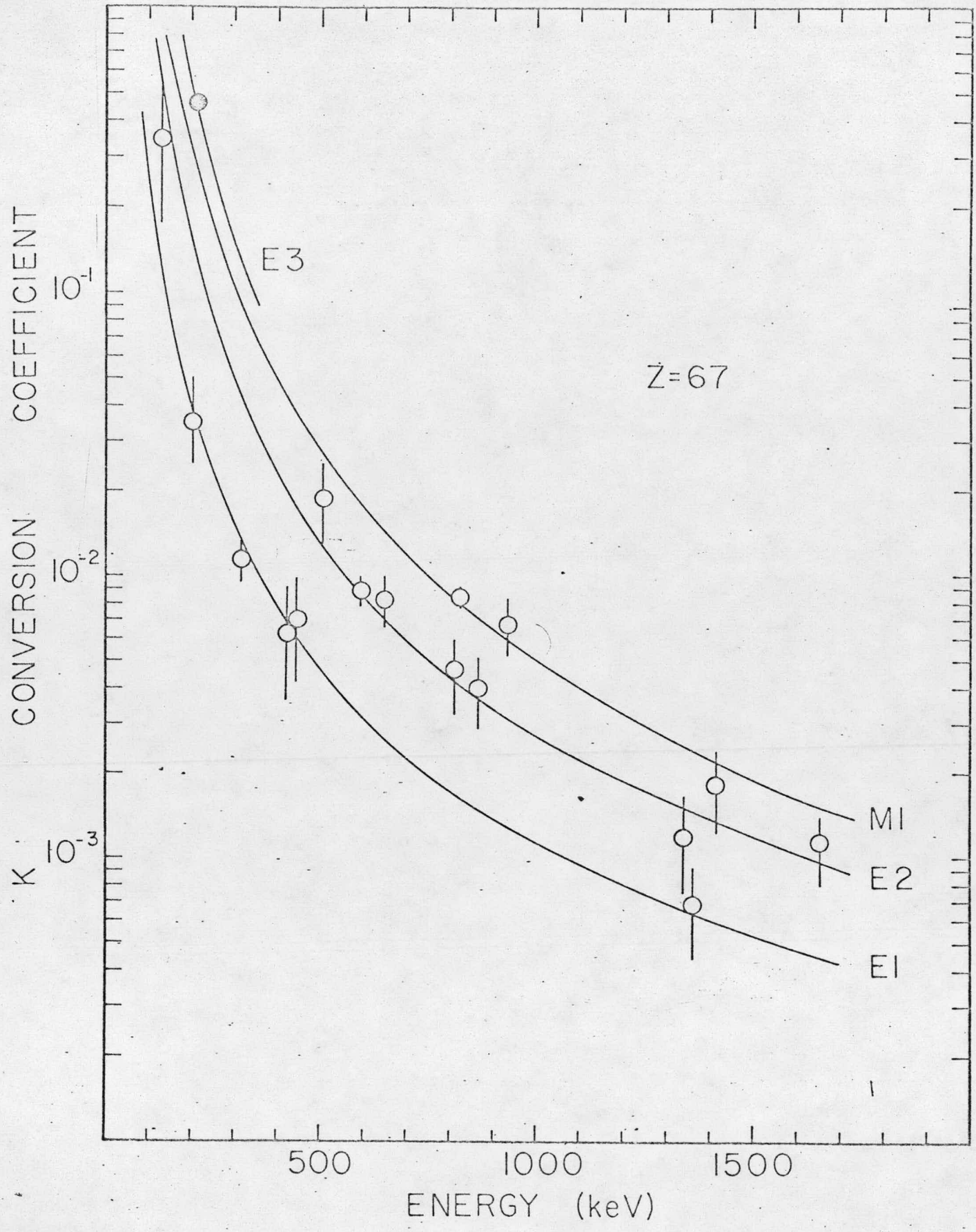
K CONVERSION COEFFICIENT
10^{-1}
10^{-2}
10^{-3}
E3
Z=67
M1
E2
E1
500
1000
1500
ENERGY (keV)

Fig 3

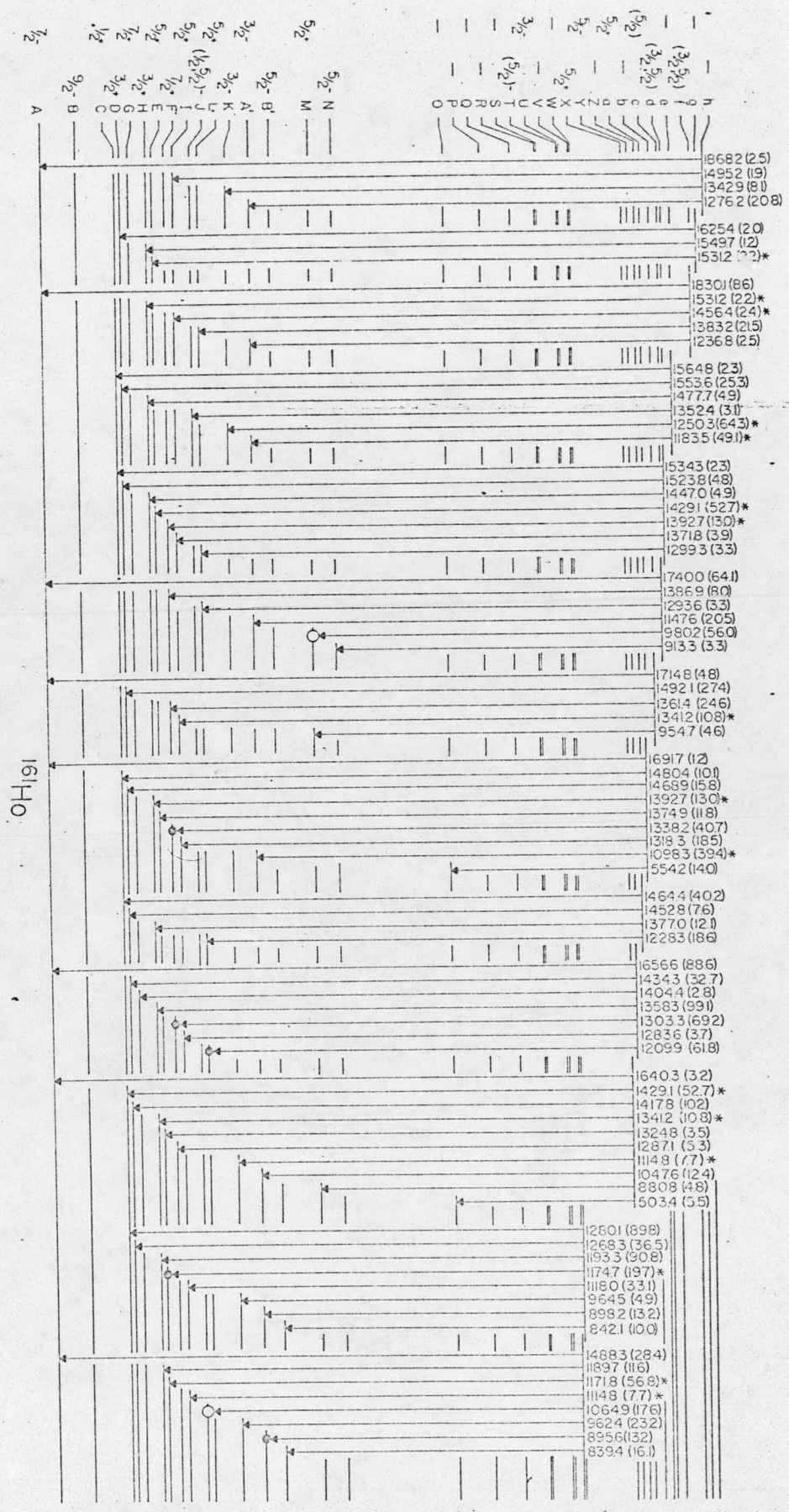
161Ho
A 7/2-
B 9/2-
C 3/2+
D 9/2+
G 3/2+
H 3/2+
E 7/2+
F 5/2+
I 5/2+
J (1/2,5/2)-
L 5/2+
K 3/2-
A' 5/2-
B' 5/2-
M 5/2-
N 5/2-
O
P
R
S (5/2)-
T
V 3/2-
W 5/2+
X 5/2+
Y 5/2+
Z (5/2)
a (3/2,5/2)+
b 5/2+
c (3/2,5/2)
d (3/2,5/2)
e
f (3/2,5/2)
g
h
18682 (2.5)
14952 (19)
13429 (81)
12762 (208)
16254 (20)
15497 (12)
15312 (22)*
18301 (86)
15312 (22)*
14564 (24)*
13832 (21.5)
12368 (2.5)
15648 (23)
15536 (25.3)
14777 (49)
13524 (31)
12503 (643)*
11835 (49.1)*
15343 (23)
15238 (48)
14470 (4.9)
14291 (52.7)*
13927 (130)*
13718 (3.9)
12993 (3.3)
17400 (64.1)
13869 (80)
12936 (3.3)
11476 (205)
9802 (560)
9133 (3.3)
17148 (48)
14921 (274)
13614 (246)
13412 (108)*
9547 (46)
16917 (12)
14804 (10.1)
14689 (15.8)
13927 (130)*
13749 (11.8)
13382 (40.7)
13183 (185)
10983 (394)*
5542 (140)
14644 (40.2)
14528 (7.6)
13770 (12.1)
12283 (18.6)
16566 (88.6)
14343 (32.7)
14044 (2.8)
13583 (99.1)
13033 (69.2)
12836 (3.7)
12099 (61.8)
16403 (3.2)
14291 (52.7)*
14178 (10.2)
13412 (108)*
13248 (3.5)
12871 (5.3)
11148 (7.7)*
10476 (12.4)
8808 (4.8)
5034 (5.5)
12801 (69.8)
12683 (36.5)
11933 (90.8)
11747 (19.7)*
11180 (33.1)
9645 (4.9)
8982 (13.2)
8421 (10.0)
14883 (28.4)
11897 (11.6)
11718 (56.8)*
11148 (7.7)*
10649 (17.6)
9624 (23.2)
8956 (13.2)
8394 (16.1)

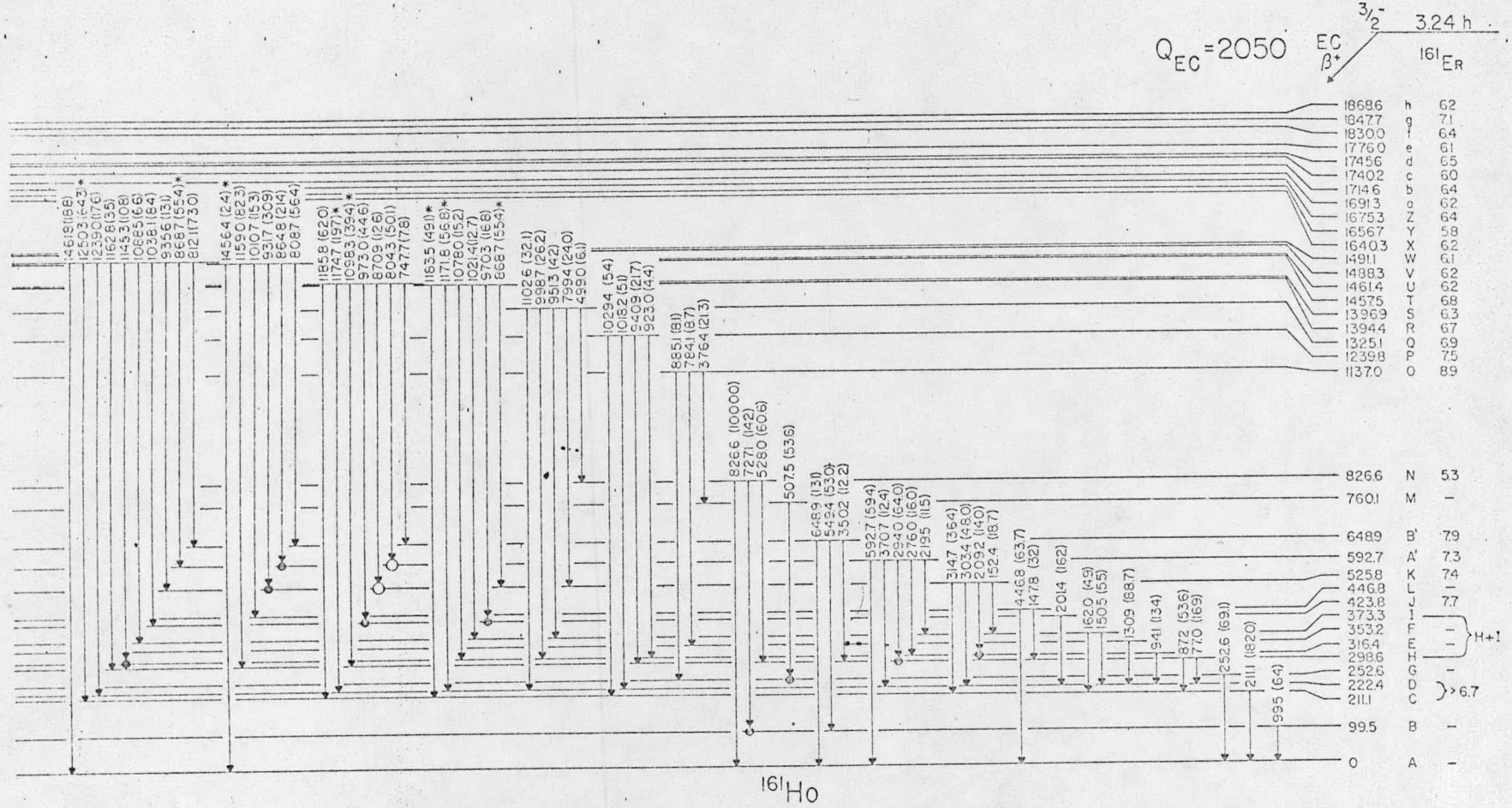
Q_EC=2050
EC
β+
3/2⁻
3.24 h
161Er
18686 h 62
18477 g 7.1
18300 f 6.4
17760 e 6.1
17456 d 6.5
17402 c 6.0
17146 b 6.4
16913 a 6.2
16753 Z 6.4
16567 Y 5.8
16403 X 6.2
14911 W 6.1
14883 V 6.2
14614 U 6.2
14575 T 6.8
13969 S 6.3
13944 R 6.7
13251 Q 6.9
12398 P 7.5
11370 O 8.9
8266 N 5.3
7601 M –
6489 B' 7.9
5927 A' 7.3
5258 K 7.4
4468 L –
4238 J 7.7
3733 I –
3532 F –
3164 E –
2986 H –
2526 G –
2224 D
2111 C
995 (64)
995 B –
0 A –
H+I 6.7
>6.7
4618 (68)
12502 (43)*
12390 (176)
11628 (135)
11453 (108)
10825 (66)
10381 (84)
9356 (131)
8697 (554)*
812 (1730)
4564 (24)*
11590 (623)
10107 (153)
9317 (309)
8648 (214)
8087 (564)
11858 (620)
11747 (197)*
10983 (394)*
9730 (446)
8709 (126)
8043 (501)
7477 (78)
11535 (491)*
11718 (568)*
10780 (152)
10214 (127)
9703 (168)
8667 (554)*
11026 (321)
9987 (262)
9513 (42)
7994 (240)
4990 (61)
10294 (54)
10162 (51)
9409 (217)
9230 (44)
8851 (81)
7841 (87)
3764 (213)
8266 (10000)
7271 (142)
5280 (606)
5075 (536)
6489 (131)
5494 (530)*
3502 (122)
5927 (594)
3707 (124)
2940 (640)
2760 (160)
2195 (115)
3147 (364)
3034 (480)
2092 (140)
152.4 (18.7)
4468 (63.7)
1478 (32)
2014 (162)
1620 (49)
1505 (55)
1309 (68.7)
941 (134)
872 (536)
770 (169)
252.6 (69.1)
211.1 (820)
161Ho

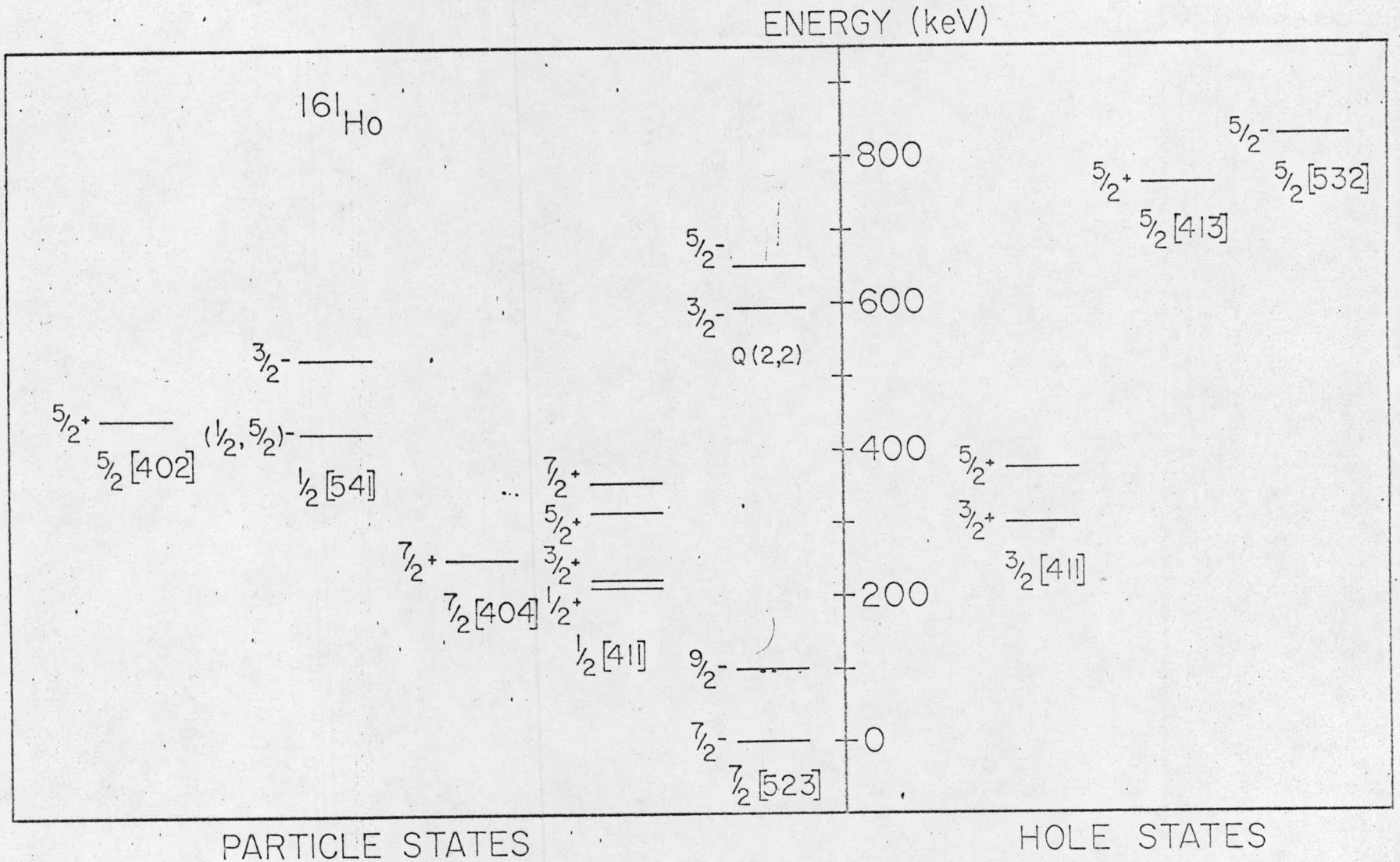
ENERGY (keV)
161Ho
800
600
400
200
0
5/2- 5/2[532]
5/2+ 5/2[413]
5/2-
3/2-
Q(2,2)
3/2-
5/2+ 5/2[402]
(1/2,5/2)- 1/2[541]
7/2+
5/2+
3/2+
1/2+
7/2+ 7/2[404]
1/2[411]
9/2-
7/2- 7/2[523]
5/2+
3/2+ 3/2[411]
PARTICLE STATES
HOLE STATES

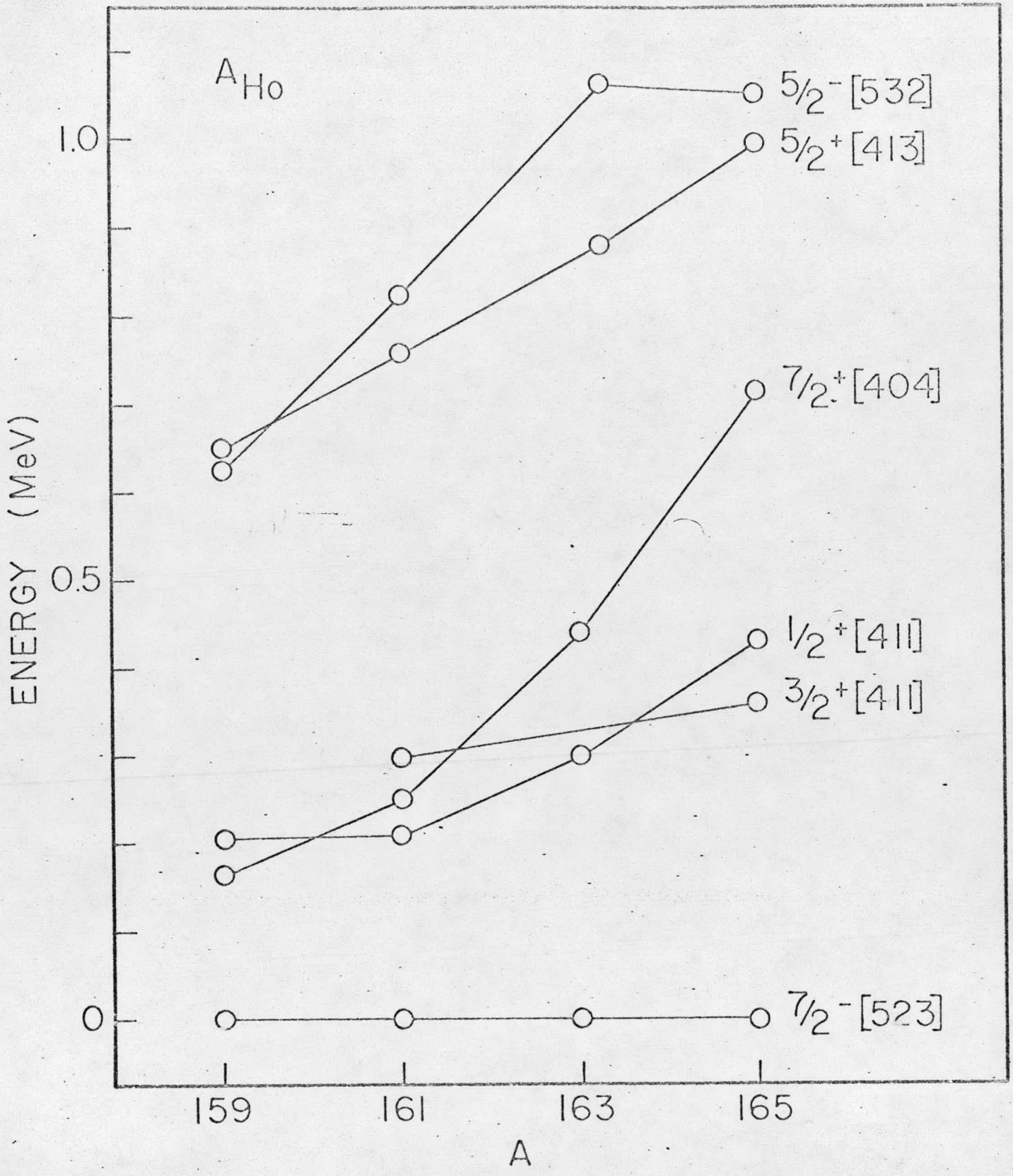
A Ho
5/2⁻ [532]
5/2⁺ [413]
7/2⁺ [404]
1/2⁺ [411]
3/2⁺ [411]
7/2⁻ [523]
ENERGY (MeV)
1.0
0.5
0
159
161
163
165
A

Fig 6

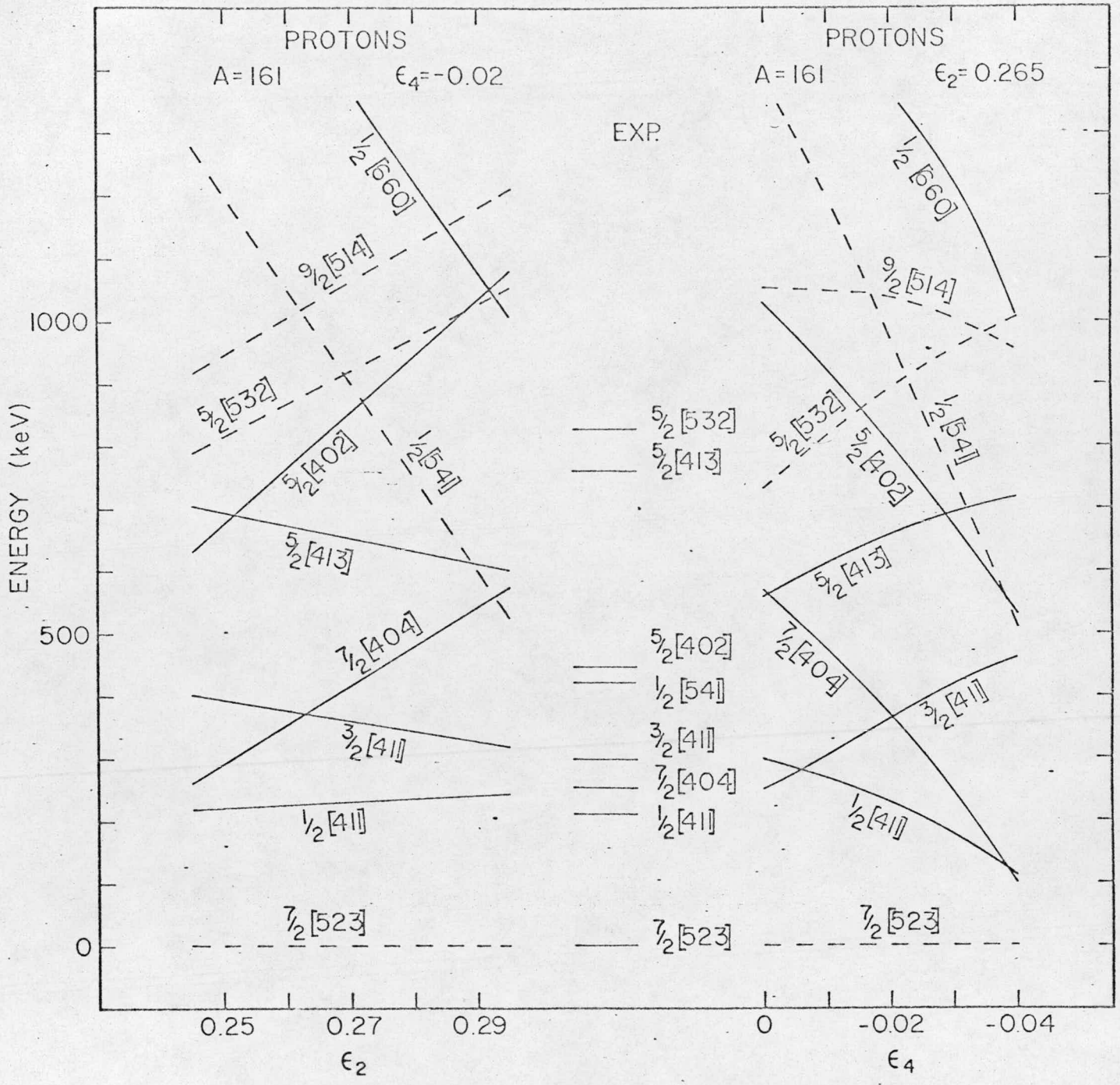
PROTONS
A=161
ϵ_4=-0.02
PROTONS
A=161
ϵ_2= 0.265
EXP.
ENERGY (keV)
1000
500
0
1/2[660]
9/2[514]
5/2[532]
5/2[402]
1/2[541]
5/2[413]
7/2[404]
3/2[411]
1/2[411]
7/2[523]
0.25
0.27
0.29
ϵ_2
0
-0.02
-0.04
ϵ_4

Fig 7

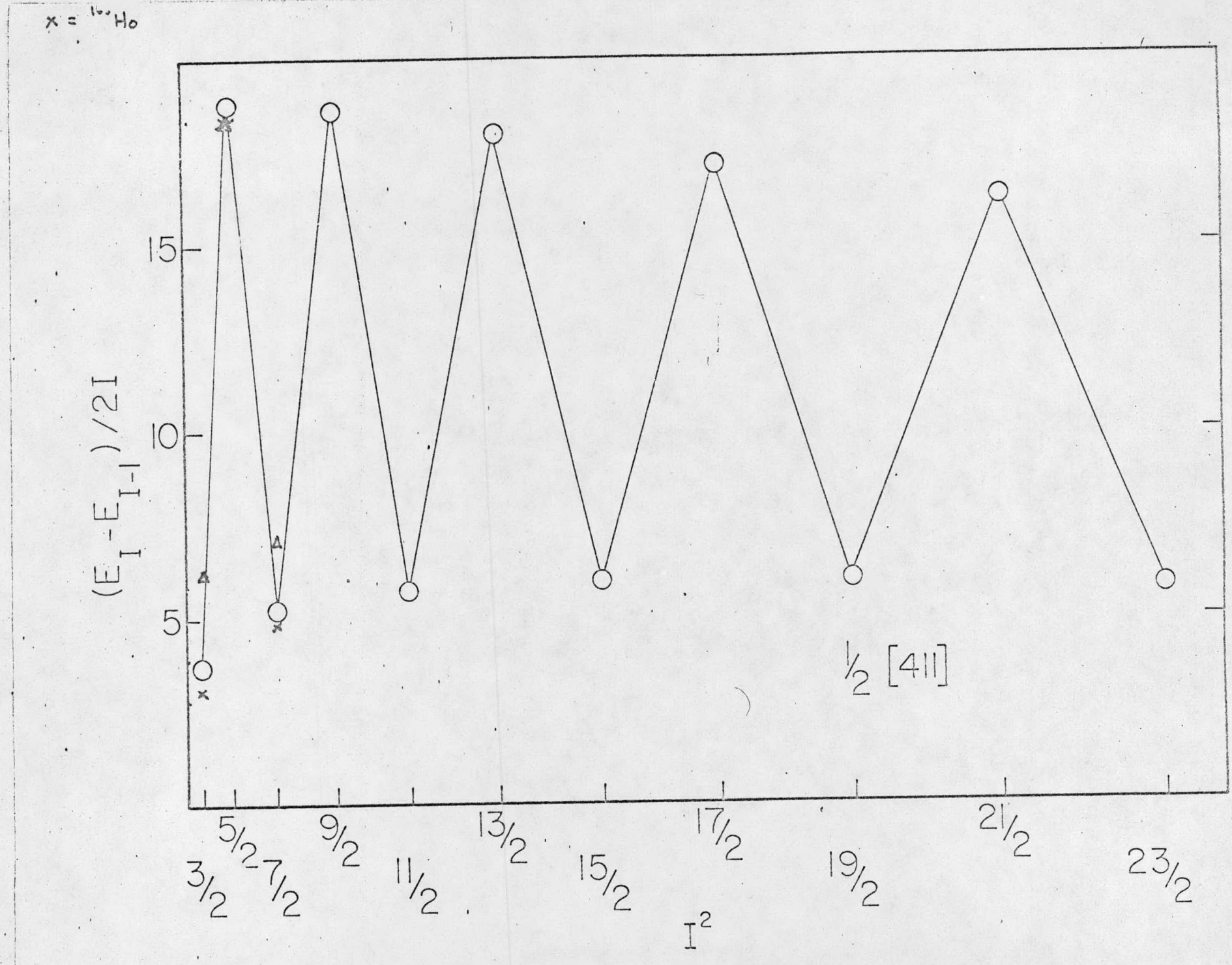
X = 165Ho
15
10
5
(E_I - E_I-1) /2I
1/2 [411]
3/2
5/2
7/2
9/2
11/2
13/2
15/2
17/2
19/2
21/2
23/2
I²

Fig 8